International Journal of Fracture **111:** 327–342, 2001.

Ductile fracture of two-dimensional cellular structures

Dedicated to Prof. Dr.-Ing. D. Gross on the occasion of his 60th birthday

I. SCHMIDT[1] and N. A. FLECK[2]
[1]*Institut für Mechanik, Technische Universität Darmstadt, D-64289 Darmstadt, Germany; (e-mail: i.schmidt@mechanik.tu-darmstadt.de)*
[2]*Cambridge University Engineering Department, Centre for Micromechanics, Trumpington Street, Cambridge CB2 1PZ, U.K.*

Received 27 November 2000; accepted in revised form 13 May 2001

Abstract. Crack growth initiation and subsequent resistance to propagation are explored numerically for regular and irregular hexagonal honeycomb structures made from ductile cell walls. The elasto-plastic response of the cell walls is described by a bilinear uniaxial stress-strain law, with fracture of the cell walls characterised by the fracture energy per unit area. Estimates for the macroscopic toughness and the associated plastic zone shape are derived analytically on the basis of simple considerations. Crack propagation is simulated numerically by fracturing elements within a finite element model and K-resistance curves are calculated under the assumption of small-scale yielding. The dependence of the crack growth behaviour upon the cell wall material parameters and geometric imperfections of the structure is investigated.

Key words: Crack propagation, crack resistance, ductile fracture, honeycombs, metal foams, numerical simulation.

1. Introduction

Cellular materials have unique property profiles, with potential for engineering use in a number of structural, thermal and acoustic applications. For example, aluminium foams are considered for structural components such as sandwich cores and for the cores of energy-absorbing tubes in automobile suspensions. Recently, the mechanical properties of cellular materials have been reviewed in the monographs of Gibson and Ashby (1998) and Ashby et al. (2000).

Regarding the fracture properties of these low density materials, previous theoretical studies have been confined to *brittle* cellular solids and to the prediction of a critical stress-intensity factor. Estimates of K_c for brittle foams and hexagonal honeycombs have been derived by Gibson and Ashby (1998) by calculating the bending moment in a cell wall adjacent to the macroscopic crack tip from the asymptotic singular stress field of linear elasticity-theory. The local stresses associated with bending of the cell walls can then be expressed in terms of the applied K, and the fracture strength of the cell wall determines K_c. In similar fashion, the fracture toughness of brittle foams with a negative Poisson ratio has been calculated and has been reported to be higher than that of conventional foams (Choi and Lakes, 1996). Chen and Huang (1998) have proposed a micro-polar continuum theory for 2d cellular structures with elastic cell walls and calculated the local stresses from the asymptotic crack tip fields of this strain gradient theory. Mode-II and mixed-mode loading are addressed in Hallström and Grenestedt (1997); they derived a fracture criterion in terms of the local stresses associated

I. Schmidt gratefully acknowledges financial support from the Deutsche Forschungsgemeinschaft for a postdoctoral fellowship and also the hospitality experienced at the Micromechanics Centre in Cambridge.

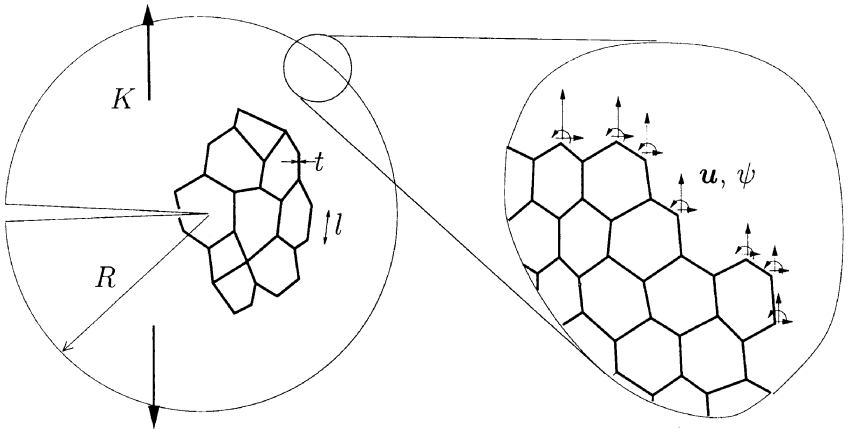

Figure 1. Cellular structure with a macroscopic crack under small scale yielding conditions. The nodal displacements and rotations are prescribed on the outer boundary.

with a continuum solution. The knock-down in strength due to the presence of cracks of length below a few cell sizes has been studied by Huang and Gibson (1991a,b).

While the macroscopic elastic-plastic deformation behaviour of metal foams has received some attention (e.g., Deshpande and Fleck, 2000; Miller, 2000), the authors are unaware of any micromechanical studies on the influence of the cell walls' ductility upon the macroscopic fracture properties of a cellular solid. This is the objective of the present paper. To assess the role of microstructural imperfections upon the toughness of an elastic-plastic honeycomb, we consider two-dimensional regular and irregular cellular structures containing a macroscopic crack under mode-I loading and employ the assumption of small scale yielding. By introducing a local failure criterion, the initiation toughness, crack resistance curves and associated plastic zone evolution are then calculated numerically. Section 1 describes the model in detail. In Section 2, appropriate nondimensional parameters are introduced and some estimates are derived. The numerical model is described in Section 3, followed by the presentation of results in Section 4, and a discussion and concluding remarks in Sections 5 and 6, respectively.

2. Specification of the model

We consider a macroscopic crack in a two-dimensional regular or irregular hexagonal honeycomb as depicted in Figure 1. The building elements of the structure are beams of average length l which are assumed to be sufficiently slender so that their shear-compliance can be neglected compared to their bending compliance. For simplicity, the beams are taken to be of rectangular cross section with thickness t. The cell wall material is described by the uniaxial bilinear stress-strain relation

$$\begin{aligned} \epsilon &= \sigma/E && \sigma < \sigma_y, \\ \epsilon &= \sigma_y/E + (\sigma - \sigma_y)/H && \sigma > \sigma_y, \end{aligned} \tag{1}$$

in terms of the true stress σ, true strain ϵ, Young's modulus E, yield strength σ_y and constant hardening modulus H. This relation holds for stresses below the fracture strength σ_f, which marks the beginning of fracture of the cell wall material. The fracture event is not modelled in detail; rather, we assume that it affects the macroscopic fracture response of the structure only through the amount of work that is dissipated due to the fracture of a beam. This means that

the fracture properties of the cell wall material are taken to be described sufficiently through the fracture energy per unit area of beam cross-section, Γ_0.

Under conditions of small-scale yielding, the displacements on a boundary remote from the crack tip are specified by the mode-I K-field. These displacements serve as boundary data with the applied K acting as a loading parameter. Macroscopic crack propagation is simulated by first incrementally increasing the displacements of the remote boundary (which is taken to be of circular shape) until the stress in one of the beams near the crack tip attains the fracture strength. Since there is no transverse distributed loading on the beams, the bending moment is linear over each beam and fracture occurs at one of the end points. Subsequently, this beam is disconnected from the respective joint in such a way that the energy dissipated during that process equals the energy dissipated through plastic deformation in the whole structure plus the work of fracture, $\Gamma_0 A$, required to drive a crack through the beam's cross section A. Within the finite element model, this local fracture process is simulated by removing an element from the discretised structure using an internal ABAQUS routine. This routine replaces the respective element with the axial- and transverse forces and the bending moment it exerts on its neighbouring nodes, and then ramps down these forces to zero; the applied K is increased during this fracture event so that the work of fracture at the failed joint equals the desired value $\Gamma_0 A$.

3. Non-dimensionalisation and estimates

Dimensional analysis reveals that the dimensionless crack growth resistance, to be made precise shortly, depends upon the following set of dimensionless parameters

$$\rho = t/l\ , \quad \sigma_y/E\ , \quad \sigma_f/\sigma_y\ , \quad H/E\ , \quad \tilde{\Gamma}_0 = \Gamma_0 E/(\sigma_y^2 l)\ , \tag{2}$$

where $\rho = t/l$, up to a factor of proportionality, can be interpreted as the relative density of the honeycomb; $\tilde{\Gamma}_0$ is, up to a constant factor, the work required to break a beam divided by the elastic strain energy contained in a beam under pure bending when the yield strain is attained at the outer fibres.

3.1. Estimate of the fracture toughness

In order to obtain a dimensionless measure of K, we derive a characteristic fracture toughness of the honeycomb as follows[1]. An order-of-magnitude estimate for the transverse deflection w of a representative beam end-point at a distance l from the macroscopic crack tip is obtained from the asymptotic K-field for a homogeneous elastic solid, giving

$$w \propto \frac{K}{E^*}\sqrt{l}\ , \tag{3}$$

where E^* is the effective Young's modulus of the honeycomb. According to Euler–Bernoulli beam theory, this displacement scales with the bending moment M, the length l of the beam and its cross-sectional dimensions b and t via

$$w \propto \frac{Ml^2}{Ebt^3}\ , \tag{4}$$

[1]The following derivation is similar that given by Gibson and Ashby (1998).

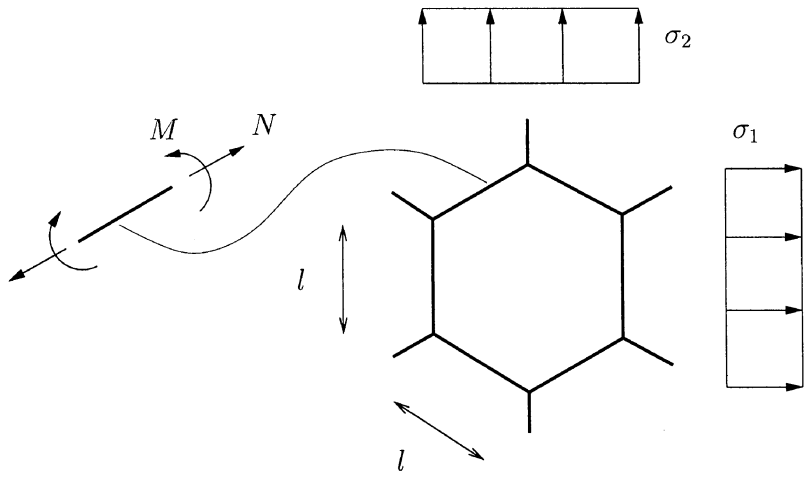

Figure 2. Regular honeycomb: macroscopic stresses and internal section forces.

where E is Young's modulus of the cell wall material. Further, the maximum stress in a beam $\sigma_{\max}$ is related to the bending moment M via

$$\sigma_{\max} \propto \frac{M}{bt^2} . \tag{5}$$

Upon combining (3), (4), (5), we arrive at

$$K \propto \sqrt{l}\,\sigma_{\max}(l/t)E^*/E . \tag{6}$$

Now, the ratio of Young's modulus of the honeycomb E^* to that of the cell walls E scales with the relative density as $E^*/E \propto (t/l)^3$ (Gibson and Ashby, 1998), and so

$$K \propto \sqrt{l}\,\sigma_{\max}(t/l)^2 . \tag{7}$$

A characteristic toughness K_Y is then obtained by equating $\sigma_{\max}$ to the yield strength of the cell wall material σ_y to give

$$K_Y = \sqrt{\pi l}\,\sigma_y(t/l)^2 , \tag{8}$$

where the factor $\sqrt{\pi}$ has been introduced for convenience. This quantity is an estimate for the stress intensity factor that causes initial yielding. An estimate for the initiation toughness could likewise be obtained by setting $\sigma_{\max}$ equal to the fracture strength σ_f to give $K_f = \sigma_f/\sigma_y K_Y$. Clearly, the proportionality relations (4) and (5) assume a linear elastic response and cease to hold once yielding has begun. Moreover, the starting point (3) is questionable even in the elastic case. However, we may still choose K_Y to make the applied K dimensionless,

$$\tilde{K} = K/K_Y \tag{9}$$

and the results presented later will show that this choice is appropriate.

3.2. Estimate of the plastic zone size and shape

3.2.1. *Regular honeycomb*

For a fully dense elastic-plastic solid, a simple estimate for the size and shape of the plastic zone around the crack tip can be obtained by checking for the satisfaction of yield using

the asymptotic elastic stress field and thereby defining a contour inside of which the stresses exceed the yield value. The same approach can be adopted for a regular honeycomb since an expression for the yield function can be easily derived, as follows. Consider the bending moment M and axial force N in a cell wall of a regular hexagonal structure subjected to macroscopic principal stresses σ_1 and σ_2 (Figure 2). From elementary considerations it follows that

$$\begin{aligned} M(\sigma_1, \sigma_2) &= \pm\tfrac{3}{8} bl^2(\sigma_1 - \sigma_2), \\ N(\sigma_1, \sigma_2) &= \tfrac{\sqrt{3}}{4} bl(3\sigma_1 + \sigma_2). \end{aligned} \tag{10}$$

If we assume that the deformation of a representative is bending dominated, the maximum stresses in the beam are given by

$$\sigma_{\max} = \left| \frac{6M}{bt^2} \right| , \tag{11}$$

and yielding occurs when this stress reaches the yield strength of the material, which, using (10), leads to the yield function

$$f(\sigma_1, \sigma_2) = |\sigma_1 - \sigma_2| - \tfrac{4}{9}\rho^2\sigma_y = 0 . \tag{12}$$

Relation (12) is a good approximation to the yield function derived by Gibson and Ashby (1998): they argued that hydrostatic loading leads to cell wall stretching and to a much higher strength than that associated with cell wall bending under deviatoric loading.

The asymptotic principal stresses for mode-I loading in plane stress are given by

$$\begin{aligned} \sigma_1(r, \varphi) &= \frac{K}{\sqrt{2\pi r}}(1 + \sin(\varphi/2)) \cos(\varphi/2), \\ \sigma_2(r, \varphi) &= \frac{K}{\sqrt{2\pi r}}(1 - \sin(\varphi/2)) \cos(\varphi/2), \end{aligned} \tag{13}$$

in terms of the polar co-ordinates (r, φ) centred on the crack tip. Upon inserting these expressions into (12) and using the definition (8), we deduce that the contour of the plastic zone is estimated by

$$r_p(\varphi)/l = 2.53\tilde{K}^2 \sin^2 \varphi . \tag{14}$$

The graph of (14) is shown in Figure 3 (innermost contour, labelled $\omega = 0$ and $\kappa = 1$)[2]; its extent in the x- and y-directions are

$$|x_p^{\max}/l| = 0.97\tilde{K}^2 , \qquad |y_p^{\max}/l| = 2.53\tilde{K}^2 . \tag{15}$$

3.2.2. *Irregular honeycomb*

Consider an irregular honeycomb as generated by displacing the vertices of a regular honeycomb by a fixed amount in random directions. The macroscopic yield function for this microstructure cannot be derived analytically. However, numerical studies show that the yield function is elliptical in deviatoric stress versus mean stress space, to a good approximation (Chen et al., 1999). In 2D, the mean stress σ_m and deviatoric stress σ_d can be expressed in terms of the principal stresses (σ_1, σ_2) as

[2]The parameters ω and κ are defined in the following section.

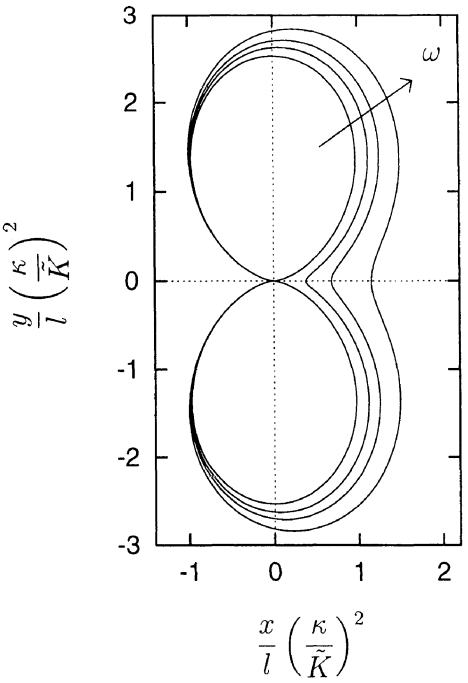

Figure 3. Estimated plastic zone shape for irregular honeycombs with ratio of uniaxial to hydrostatic yield strength of $\omega = 0., 0.7, 0.8, 0.9$.

$$\sigma_m = \tfrac{1}{2}(\sigma_1 + \sigma_2)\,, \qquad \sigma_d = \tfrac{\sqrt{2}}{2}|\sigma_1 - \sigma_2|\,, \tag{16}$$

and the yield function $f(\boldsymbol{\sigma})$ has the form

$$f(\sigma_1, \sigma_2) = \sigma_d^2 + \beta^2\sigma_m^2 - Y^2 = 0\,, \tag{17}$$

where β describes the shape of the yield surface and Y is its overall size. This functional form with $\beta \approx 1$ reflects the fact that, in an irregular honeycomb of sufficiently low relative density, cell wall bending dominates stretching under all loading states (see, e.g., Chen et al., 1999). The strength Y is related to the uniaxial yield strength of the irregular honeycomb σ_u by

$$Y = \tfrac{1}{2}\sqrt{2+\beta^2}\sigma_u\,, \tag{18}$$

and the parameter β is related to the ratio of uniaxial to hydrostatic yield strength $\omega \equiv \sigma_u/\sigma_h$ via

$$\beta^2 = \frac{2\omega^2}{4-\omega^2}\,. \tag{19}$$

Proceeding as before, we arrive at the following estimate for the contour of the plastic zone:

$$r_p(\varphi)/l = \frac{5.06}{2+\beta^2}\frac{\tilde{K}^2}{\kappa^2}[\sin^2(\varphi/2) + \beta^2(1+\cos\varphi)], \tag{20}$$

in which κ denotes the ratio of uniaxial yield strength for the irregular and regular honeycombs. Figure 3 depicts the shape given by (20) for selected values of ω in the range 0 to 0.9; for a typical metallic foam $\omega \approx 0.9$ (cf., Deshpande and Fleck, 2000). Increasing ω corresponds to a reduced hydrostatic yield strength; this causes the plastic zone to extend directly ahead of the crack tip where the stress state is purely hydrostatic while the overall

dimensions of the plastic zone are essentially left unchanged. For the limiting case $\omega = \beta = 0$ and $\kappa = 1$, the result (14) is recovered.

4. Numerical technique

For the numerical evaluation of the model described in Section 2, a finite element method is used to calculate stresses and strains in the cell walls of a honeycomb bounded by a circle of radius $R \approx 85l$. This value has been found to give converged results. The cell walls are modelled by Euler–Bernoulli beams which are discretised with up to 7 cubic beam elements whose material behaviour is defined by (1). The displacements u_i and rotations ψ of the beam ends are prescribed on the outer boundary (see Figure 1) according to the asymptotic field

$$\begin{aligned} u_1(r,\varphi) &= \frac{K\sqrt{r}}{2\mu^*\sqrt{2\pi}} \cos\varphi/2(\alpha - \cos\varphi) \\ u_2(r,\varphi) &= \frac{K\sqrt{r}}{2\mu^*\sqrt{2\pi}} \sin\varphi/2(\alpha - \cos\varphi) \,, \\ \psi(r,\varphi) &= \tfrac{1}{2}(u_{2,1} - u_{1,2}) \end{aligned} \tag{21}$$

where $\alpha = (3 - \nu^*)/(1 + \nu^*)$ for plane stress and μ^*, ν^* are the effective shear modulus and Poisson ratio of the honeycomb, given in terms of the relative density measure $\rho \equiv t/l$ by (cf., Gibson and Ashby, 1998)

$$\mu^* = \frac{E^*}{2(1+\nu^*)} \,, \qquad E^* = E\frac{4}{\sqrt{3}}\frac{\rho^3}{1+3\rho^2} \,, \qquad \nu^* = \frac{1-\rho^2}{1+3\rho^3} \,. \tag{22}$$

The structure is loaded up to the point where the fracture strength σ_f is reached in one of the beams; the respective element is then removed from the model, thereby disconnecting the fractured beam from a vertex. As mentioned earlier, this element removal is performed with a built-in routine of the finite element code ABAQUS which first replaces the element with the forces and moments it exerts on its neighbouring nodes and subsequently reduces these section forces to zero *over a prescribed load-parameter interval*. This interval, i.e. the change in the applied stress-intensity factor ΔK, determines a posteriori the work of fracture per unit area Γ_0 of the removed beam, which is evaluated numerically. By choosing ΔK appropriately, Γ_0 can be adjusted to the desired value. This includes the possibility of negative values of ΔK, corresponding to an unloading of the structure, and therefore allows also for R-curves with a negative slope. The crack extension Δa is then defined as the x co-ordinate of the vertex to which the failing end of the beam was connected, or the previous value of Δa, depending upon the larger of the two.

5. Results

The current study is aimed at gaining some insight into the fracture properties of metallic foams – rather than real honeycombs – and so the following cell wall material parameters are chosen as representative of those for aluminium alloy foams:

$$\sigma_y/E = 0.1\% \,, \quad \sigma_f/\sigma_y = 2.0 \,, \quad H/E = 0.1 \,, \quad \tilde{\Gamma}_0 = 3.0 \,. \tag{23}$$

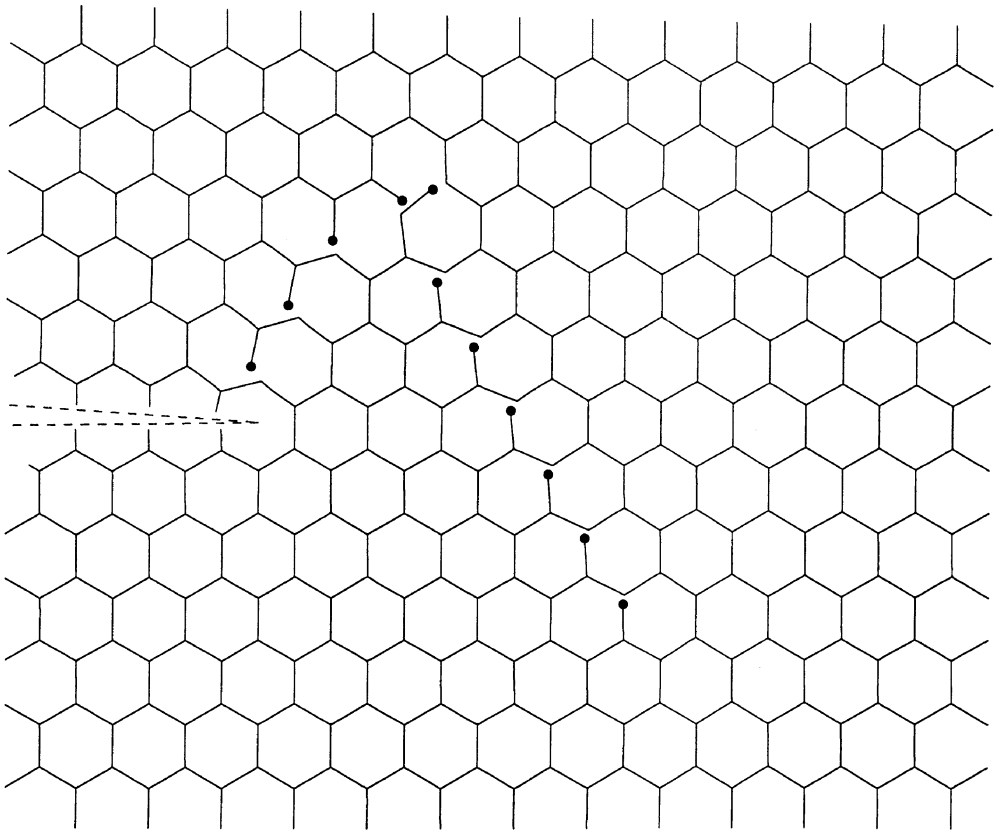

Figure 4. Predicted crack path in a regular honeycomb for the material parameters given in (23) and $\rho = 5\%$.

5.1. CRACK PATH IN REGULAR HONEYCOMB

A typical prediction of crack path is shown in Figure 4 for the case $\rho = 5\%$ with loading taken to the point where 9 cell walls have failed. The cell wall in which the fracture strength is reached first is *not* the one directly ahead of the 'crack tip'; rather, the highest bending moments are attained above and below the crack tip. As a result of the structure's regularity, the crack follows a tortuous path[3]. The beams which fail do not lay on a continuous path: they break the structure into a multiply connected domain. Consequently, some traction can still be transmitted across the zone of cracking, and the disconnected crack advance can be viewed as a bridging zone.

Figure 5 shows the plastic zones around the crack tip at initiation and at $\Delta a = 7l$ for the choice $\rho = 5\%$. The distribution of the plastic strains is illustrated by marking with crosses those vertices where at least one of the adjoining beams has undergone plastic yielding; the two different intensities of the crosses correspond to plastic strains between $0.5\epsilon_y$ and $5\epsilon_y$ and greater than $5\epsilon_y$, respectively. It can be seen that appreciable plastic strains are confined to a narrow region around the crack path. The dashed lines in these figures represent the estimate (14) for the plastic zones. While these estimates appear to be somewhat too large, this picture changes when one would mark *all* vertices with non-zero plastic strain – no matter how small. In this case the coincidence is very good (not shown).

[3]The initial symmetry about the line of the macroscopic crack is broken by disconnecting only one of the two beams in which the stress reaches the fracture strength for the first time.

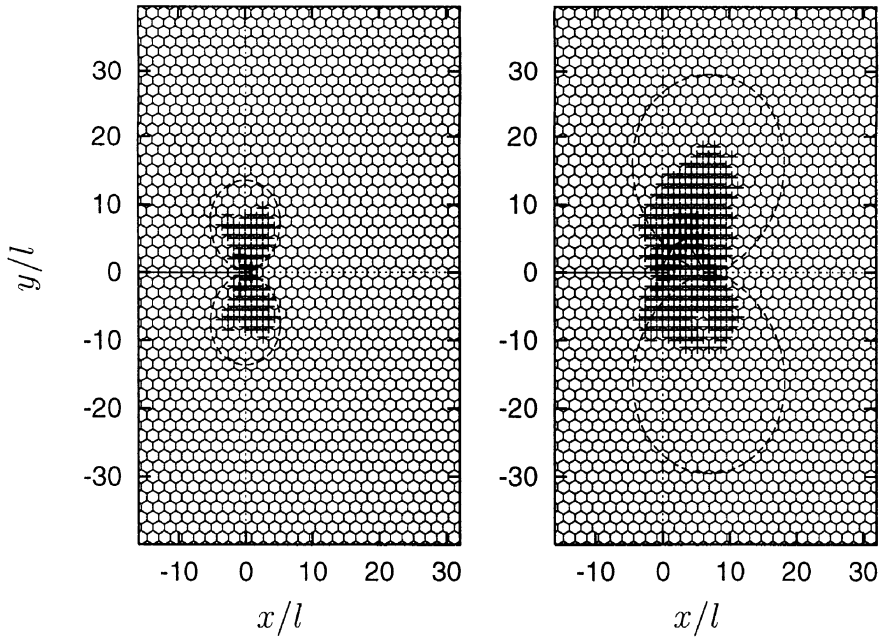

Figure 5. Plastic zones for the regular honeycomb at initiation (left) and for $\Delta a = 7l$ (right).

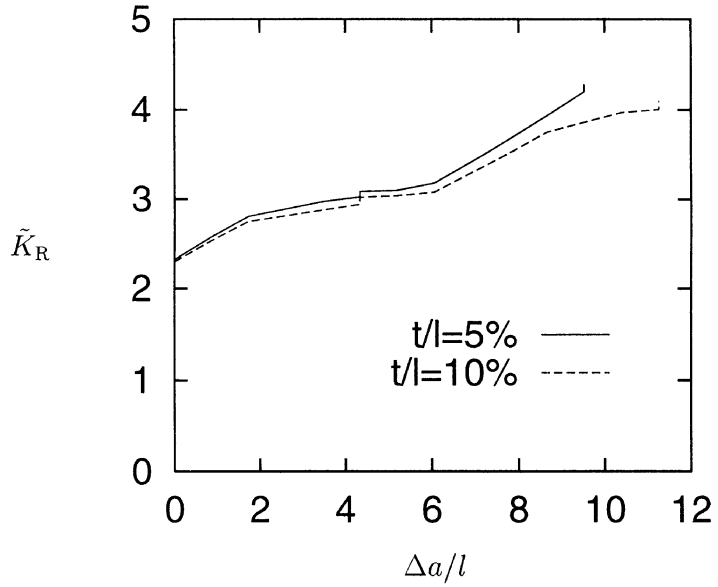

Figure 6. K-resistance curve for the regular honeycomb at two values of relative density.

The corresponding crack resistance curves for $\rho = 5\%$ and 10% are presented in Figure 6. Despite the large difference in the corresponding values of ρ, the curves differ negligibly. The absolute values of the crack resistance, however, are very different because ρ enters the non-dimensionalisation (9) for the stress intensity factor. This implies that the influence of the relative density of the honeycomb is essentially captured in (9). Moreover, the initiation toughness is approximately $K_c \approx 2.3K_Y$ which is remarkably close to the estimate $K_c = \sigma_f/\sigma_y K_Y = 2.0K_Y$ derived earlier. The crack resistance has not attained a steady-state value over the range considered here.

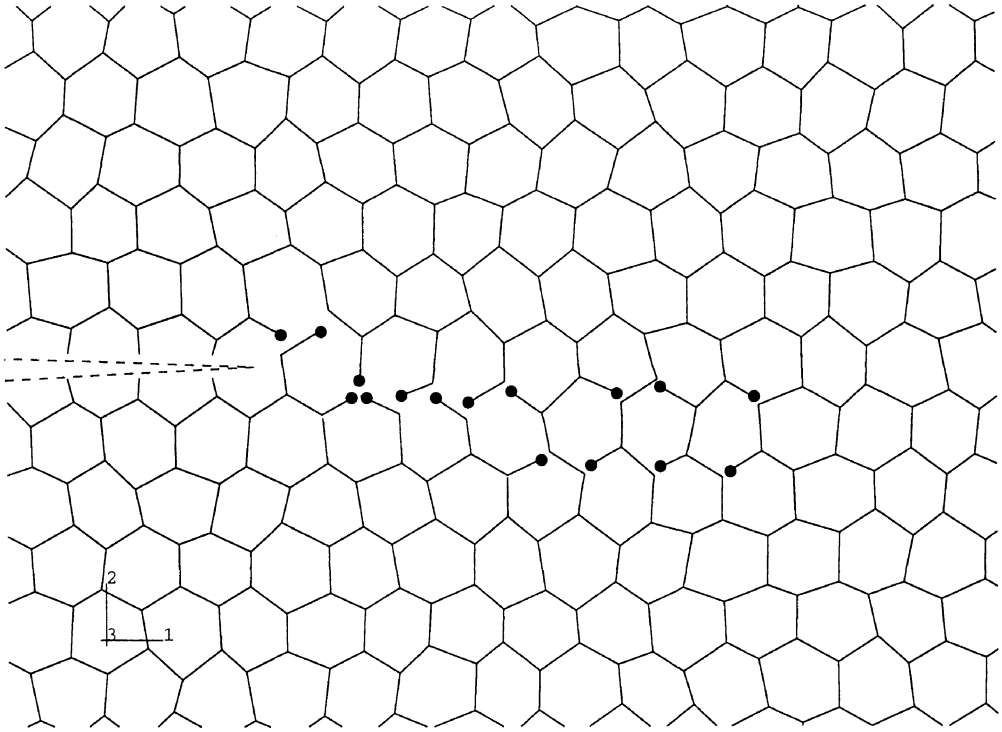

Figure 7. Predicted crack path in an irregular honeycomb.

5.2. CRACK PATH IN IRREGULAR HONEYCOMB

Next, consider the case of an irregular honeycomb. This structure is generated by randomly perturbing the vertex positions of a regular hexagonal honeycomb, the amount of perturbation being uniformly distributed between -15% and $+15\%$ of the average beam length. In order to obtain crack resistance curves a set of 5 different realisations of such structures has been analysed. The K_R values at each stage of the crack propagation are then averaged over the 5 realisations to give an averaged crack resistance. While five realisations are insufficient to give an accurate averaged response, it is believed that they provide a useful qualitative picture.

A typical pattern of crack propagation in an irregular honeycomb with the set of parameters (23) is shown in Figure 7 ($\rho = 5\%$). No oscillation of the crack path can be observed; the crack extends more or less in a self-similar direction. Also, the degree of crack bridging is less significant.

The plastic zones at initiation and at $\Delta a = 8l$ are shown in Figure 8 together with the estimate (20), in which $\omega = 0.7$ and $\kappa = 0.8$ have been used[4]. These plots have been obtained by marking with a cross the plastic vertices of the 5 realisations in the same plot. Thus, the intensity of the markers can be viewed as the ensemble average for the magnitude of the plastic strain around the crack tip. As in the case of regular honeycombs, the estimate (20) for the plastic zone is in reasonable agreement with the numerical results with regard to both shape and size.

The crack resistance curves for regular and irregular honeycombs are compared in Figure 9. The error bars indicate the standard deviation from the corresponding mean value of the

[4]These values have been extrapolated from the calculations in Chen et al. (1999) for the chosen level of imperfection in the foam.

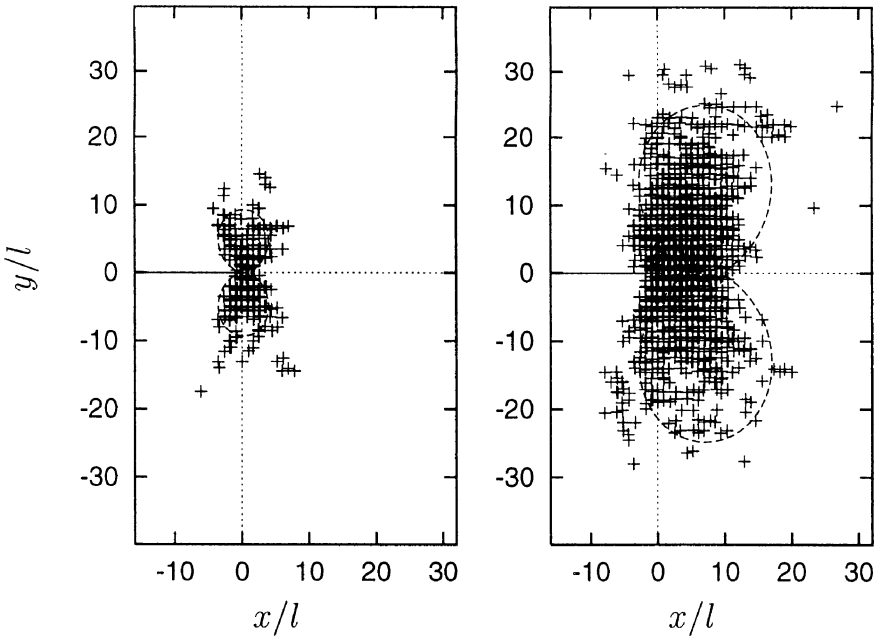

Figure 8. Plastic zones for the irregular honeycomb at initiation (left) and for $\Delta a = 8l$ (right).

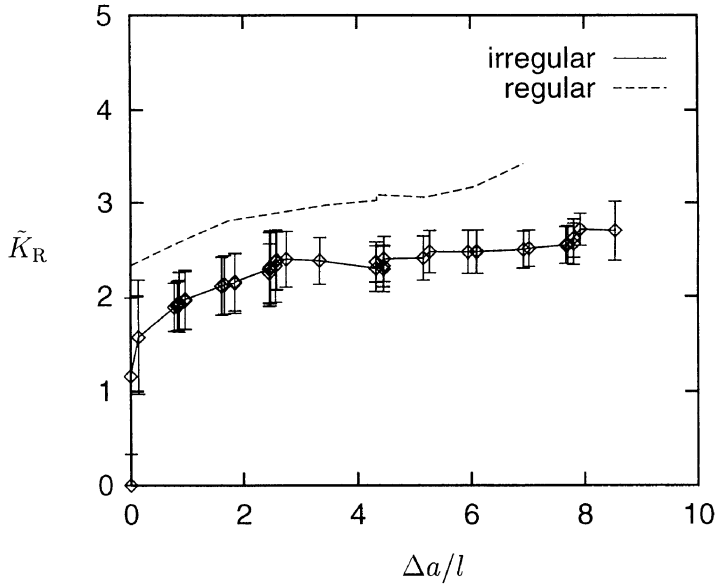

Figure 9. Comparison of the predicted K-resistance curves for regular and irregular honeycombs.

irregular structures. It is evident that the toughness is considerably reduced by the irregularity in microstructure.

5.3. Effect of cell wall properties upon macroscopic toughness

It has already been shown in Figure 6 that the effect of the relative density measure ρ upon the R-curve of the regular honeycomb is adequately captured through the choice of the normalisation $\tilde{K}$. Numerical experimentation confirmed that this also holds in the case of irregular honeycombs. Next, we explore the effect of the remaining non-dimensional cell wall properties σ_f/σ_y, H/E, σ_y/E and $\tilde{\Gamma}_0$ upon the crack resistance curve for the irregular honeycomb,

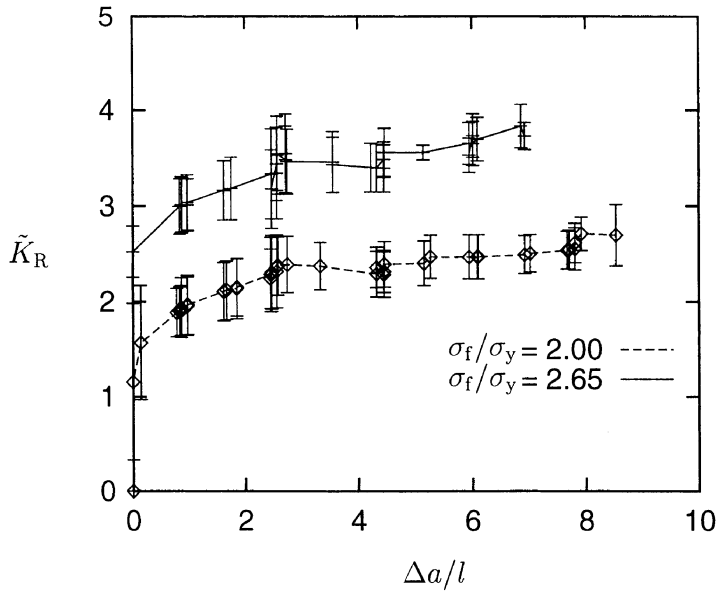

Figure 10. K-resistance curves for altered fracture strength.

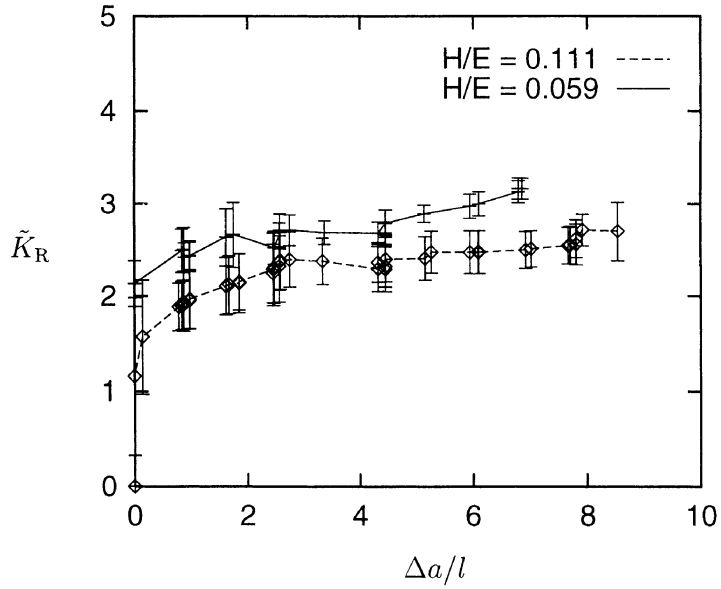

Figure 11. K-resistance curves for altered hardening modulus.

at $\rho = 5\%$. Figures 10, 11 and 12 show the crack resistance curves (in the average sense described before) for altered fracture strength ($\sigma_f/\sigma_y = 2.0 \rightarrow 2.65$), hardening modulus ($H/E = 0.11 \rightarrow 0.059$) and yield strain ($\sigma_y/E = 0.1\% \rightarrow 0.2\%$), respectively. For comparison, the baseline curve from Figure 9 is included as a dashed line in each of Figures 10–12.

We note that the curves are qualitatively similar and differ essentially through a constant shift along the K_R axis. That is, the slope of the resistance curve is much less affected by the cell wall properties than is its absolute value.

An increase of the fracture strength ratio σ_f/σ_y leads to higher K_R values (Figure 10): as might be expected, a larger applied K is needed to break the first beam. Likewise, decreasing the normalised hardening modulus H/E leads to elevated K_R values: the physical interpreta-

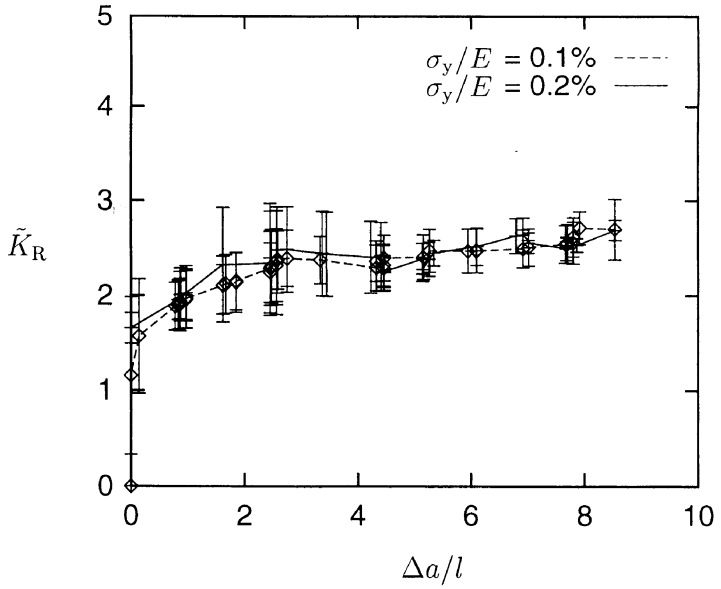

Figure 12. K-resistance curves for altered yield strain.

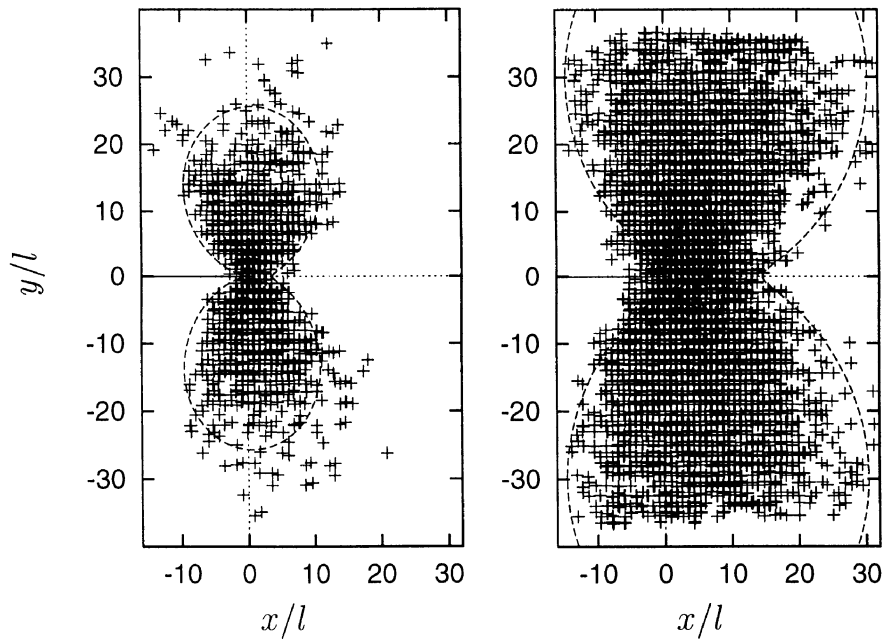

Figure 13. Plastic zones for $\sigma_f/\sigma_y = 2.65$ at initiation (left) and for $\Delta a = 7l$ (right).

tion is that a reduced hardening modulus requires a larger deformation of the mesh boundary for the stresses to reach the unaltered fracture strength (Figure 11). The response is only mildly sensitive to a change in yield strain, in contrast to the effect of H/E and of σ_f/σ_y (Figure 12).

The plastic zones corresponding to the altered values of fracture strength and hardening modulus are shown in Figures 13 and 14, together with the estimate based on (20). The same values $\omega = 0.7$ and $\kappa = 0.8$ have been used here as in Figure 8 and the accuracy of the analytical estimate of the plastic zone size remains high.

Since the shape of the resistance curves remains practically unchanged upon altering the cell wall material parameters, their influence may be characterised by calculating only the initiation toughness as a function of these parameters. Figure 15 shows that $\tilde{K}_c$ increases

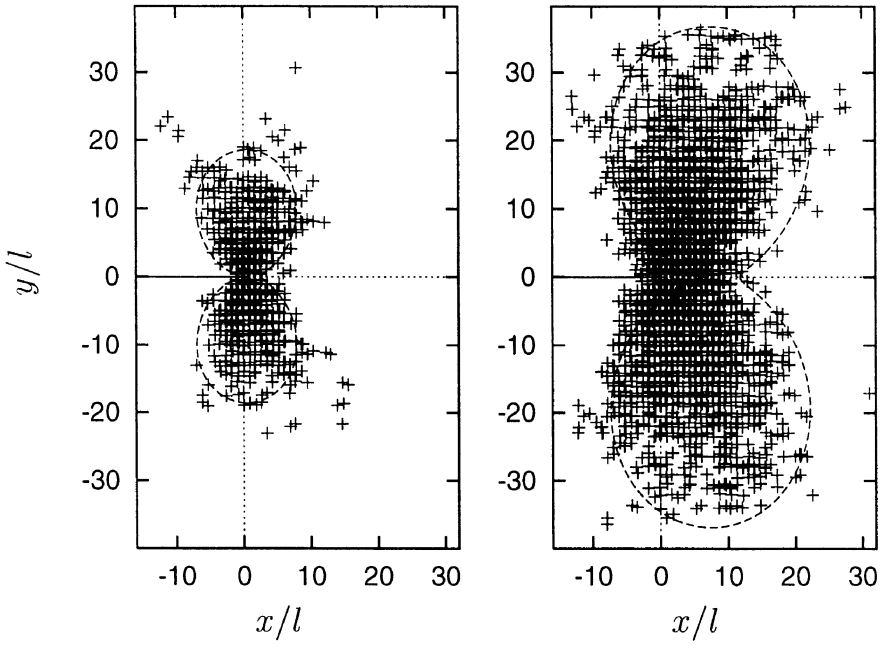

Figure 14. Plastic zones for $H/E = 0.059$ at initiation (left) and for $\Delta a = 7l$ (right).

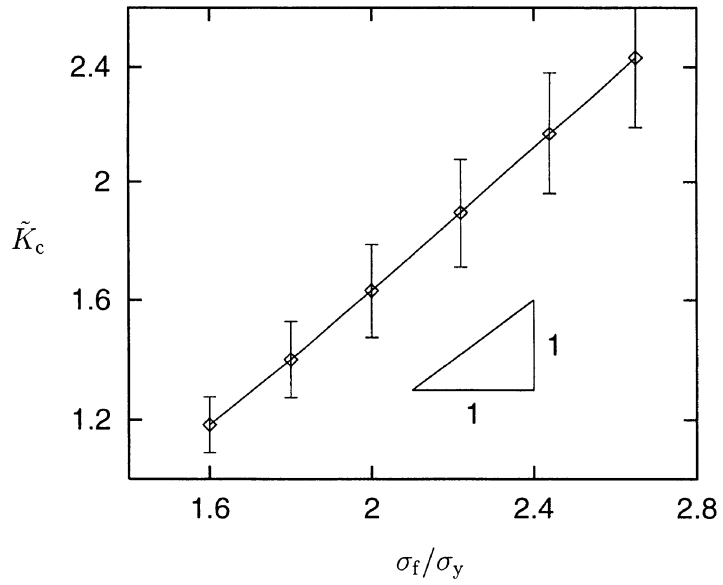

Figure 15. Initiation toughness as a function of fracture strength.

linearly with the normalised fracture strength σ_f/σ_y, with a slope of about unity; this is in line with the dependence predicted by the estimate $K_f = \sigma_f K_Y/\sigma_y$ mentioned earlier. Figure 16 depicts $\tilde{K}_c$ as a function of the hardening modulus in a log-scale representation and shows a power law dependence with an exponent of approximately $-\frac{1}{3}$. The simple estimate $K_f = \sigma_f K_Y/\sigma_y$ has no dependence upon H/E because its derivation ignores plasticity altogether.

6. Concluding remarks

Crack growth under mode-I loading and small scale yielding conditions in 2d cellular structures has been simulated numerically using a finite element method in conjunction with an

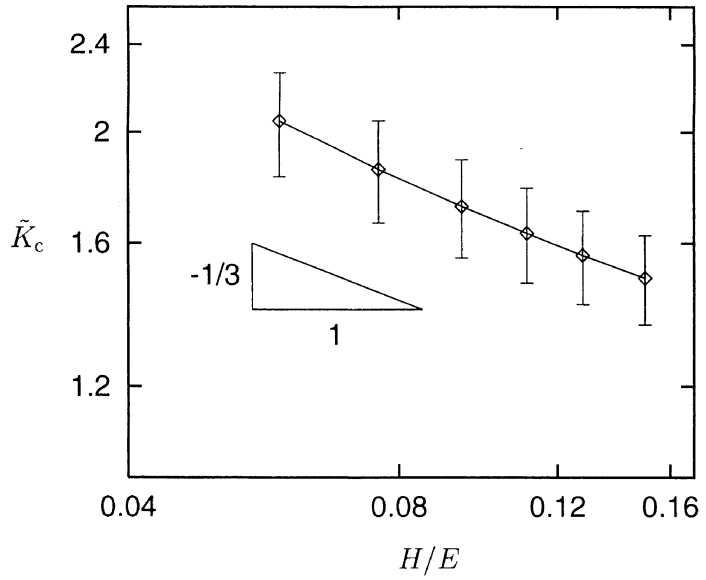

Figure 16. Initiation toughness as a function of hardening modulus.

element-removal technique. The method allows for the calculation of crack growth resistance curves, including the associated evolution of plastic zones, and their dependence on the cell wall material parameters. It is found that the crack growth resistance scales quadratically with relative density and linearly with the ratio of fracture to yield strength of the cell wall material. No significant effect of these parameters on the slope of the resistance curves was detected. Throughout this study, the fracture energy Γ_0 has been kept constant. Numerical experimentation revealed that an increase in Γ_0 leads to large changes in the applied stress intensity factor during the process of removing an element (i.e., fracture of a beam) – with the effect that, at the end of a particular removal step, the stress may have attained the fracture strength in *several* other elements. In this case, the proposed method fails to describe the process adequately since it does not allow for the sequential fracture of beams at the crack tip. Nevertheless, we conclude that the slope of the R-curve will increase with increasing Γ_0. The proposed method can in principle be applied to the three-dimensional case too. However, this would lead to very large computation times, chiefly because of the iterative computation of the change in the applied K during the fracture of a beam. It would be desirable to have a method that allows one to simulate the fracture of a beam without interrupting the computation and without the necessity to adjust ΔK so as to match the prescribed value of Γ_0. Work in this direction is underway.

The numerical results support an analytic estimate for the plastic zone size at fracture initiation: the size scales with the square of the stress intensity factor and is inversely proportional to the 4th power of the relative density.

References

Ashby, M., Evans, A., Fleck, N., Gibson, L., Hutchinson, J., and Wadley, N. (2000). *Metal Foams – a Design Guide*. Butterworth, Heinemann, Boston, USA.

Chen, C., Lu, T.J., and Fleck, N.A. (1999). Effect of imperfections on the yielding of two-dimensionals foams. *Journal of the Mechanics and Physics of Solids* **47**, 2235–2272.

Chen, J.Y. and Huang, J.S. (1998). Fracture analysis of cellular materials: a strain gradient model. *Journal of the Mechanics and Physics of Solids* **46**, 789–828.

Choi, J.B. and Lakes, R.S. (1996). Fracture toughness of re-entrant foam materials with a negative Poisson's ratio: experiment and analysis. *International Journal of Fracture* **80**, 73–83.

Deshpande, V.S. and Fleck, N.A. (2000). Isotropic constitutive models for metallic foams. *Journal of the Mechanics and Physics of Solids* **48**, 1253–1283.

Gibson, L.J. and Ashby, M.F. (1998). *Cellular Solids*. Pergamon Press, London.

Hallström, S. and Grenestedt, J. (1997). Mixed mode fracture of cracks and wedge shaped notches in expanded PVC foam. *International Journal of Fracture* **88**, 343–358.

Huang, J.S. and Gibson, L.J. (1991a). Fracture toughness of brittle foams. *Acta Metall. Mater.* **39**, 1627–1636.

Huang, J.S. and Gibson, L.J. (1991b). Fracture toughness of brittle honeycombs. *Acta Metall. Mater.* **39**, 1617–1626.

Miller, R. (2000). A continuum plasticity model of the constitutive and indentation behavior of foamed metals. *International Journal of Mechanics Sciences* **42**, 729–754.